Contents lists available at ScienceDirect

Journal of Molecular Liquids

journal homepage: http://ees.elsevier.com

High-pressure crystal polymorphs in 1-butyl-3-methylimidazolium perfluorobutanesulfonate

Yoshihiro Koyama [a], Seiya Shimono [b], Hiroaki Kishimura [b], Takahiro Takekiyo [c], Yukihiro Yoshimura [c], Hiroshi Abe [b], Kiyoto Matsuishi [a]

[a] Graduate School of Pure and Applied Science, University of Tsukuba, Tsukuba 305-8573, Japan
[b] Department of Materials Science and Engineering, National Defense Academy, Yokosuka 239-8686, Japan
[c] Department of Applied Chemistry, National Defense Academy, Yokosuka 239-8686, Japan

ARTICLE INFO

Article history:
Received 3 March 2021
Received in revised form 29 April 2021
Accepted 3 May 2021
Available online xxx

Keywords
Fluorinated ionic liquid
Crystal polymorph
Molecular conformations
Conformational flexibility

ABSTRACT

The high-pressure (HP) crystal polymorph of a fluorinated ionic liquid (fIL) was determined using X-ray diffraction and Raman spectroscopy. The irreversible crystal polymorph of 1-butyl-3-methylimidazolium perfluorobutanesulfonate ([C_4mim][PFBS]) was observed upon compression and decompression using X-ray diffraction. Conformational variance/invariance of $[C_4mim]^+$ and $[PFBS]^-$ in the Raman spectra corresponded to the HP crystal polymorph. By the degrees of freedom of the conformations and their conformational flexibilities, the conformational variance was switched at the specific pressure for a volume contraction under HP, at which point the crystal system changed. The HP crystal polymorph was entirely different from the low-temperature crystal polymorph.

1. Introduction

Crystal polymorphs are observed in molecular crystals owing to the degrees of freedom of the molecular conformations [1]. Computer-aided crystal structure prediction (CSP) supports experimentally obtained crystal polymorphs [2–4]. Furthermore, CSP is utilized in crystal polymorph screening in pharmaceuticals [5–7]. Under high pressure (HP), the physicochemical properties of pharmaceuticals are largely influenced by the crystal polymorphs. Thus, polymorph screening is an urgent issue in the pharmaceutical industry. To further develop CSP, the crystal energy landscape [8–12] has been introduced in the same manner as the free energy landscape [13] in supercooled liquids and amorphous.

Ionic liquids (ILs) have been investigated from a viewpoint of liquid structures and molecular conformations. ILs consist of a cation and an anion. Previously, the molecular conformations of 1-alkyl-3-methylimidazolium ($[C_n mim]^+$) cations have been were calculated [14–17], where *n* represents the alkyl chain length. In $[C_4mim]^+$, three stable conformations *TT*, *GT*, and *G'T* were optimized using *ab initio* calculations [15]. Also, the Raman bands of each conformer were assigned according to the calculations. Recently, the torsional potential of perfluorobutanesulfonate ($C_4F_9SO_3^-$, $[PFBS]^-$) was evaluated by density functional theory (DFT) calculations [18]. The stable conformers of $[PFBS]^-$ were found to be *trans* and *gauche*. The calculation results were similar to those of the $[C_4F_9BF_3]^-$ [19].

Phase behaviors of fluorinated ionic liquid (fILs) have been examined at low temperature (LT), using differential scanning calorimetry (DSC) [20,21]. By changing the type of the fIL cation, the complicated crystal polymorphs induced by $[PFBS]^-$ were found. The variety of crystal polymorphs for fILs could be related to their specific nano-heterogeneities in the liquid state of fILs [22]. The crystal structures of 1,2,4-triazolium [PFBS] were determined using single-crystal X-ray diffraction [23]. Despite the simple molecular structure of the cation, the crystal structures had large lattice constants. In the unit cell, the *trans* conformer of $[PFBS]^-$ was formed, and the non-negative charge distribution of the perfluorobutyl chains in $[PFBS]^-$ contributed to the long crystallographic *c*-axis, which was preferred molecular packing. Very recently, the LT crystal structures of [$C_n$mim][PFBS] (n = 4, 6, and 8) were determined using simultaneous X-ray diffraction and DSC measurements [18]. The *trans* conformer of $[PFBS]^-$ existed in the unit cell of [C_4mim][PFBS], and the crystals of [$C_n$mim][PFBS] (n = 4, 6, and 8) possessed long lattice constants at LT. Moreover, the crystal polymorphs of the fILs became proportionally more complicated with the length of the alkyl chain length in $[C_n mim]^+$.

In this study, the phase behaviors of [C_4mim][PFBS] were investigated under HP. The HP crystal polymorph of the fIL was measured using X-ray diffraction and Raman spectroscopy. The complicated and irreversible HP crystal polymorph was determined by the degrees of freedom of the cationic and anionic conformers, and their conformational flexibility.

https://doi.org/10.1016/j.molliq.2021.116415
0167-7322/

2. Materials and methods

The fIL used in this study was [C_4mim][PFBS] (FUJIFILM Wako Pure Chemical Co.). We used the as-received samples without further purification, as vacuum contamination easily occurred.

HP X-ray diffraction experiments were performed using a Mao-Bell type diamond anvil cell (DAC) in the BL-18C of the Photon Factory at the High Energy Accelerator Research Organization in Japan [24]. In a glovebox with dry flowing nitrogen, the sample and ruby balls were loaded into the hole (0.25 mm) of the pre-indented stainless gasket with a thickness of 0.18 mm in the DAC. A microbeam with a diameter of 35 μm was obtained using double collimators. Two-dimensional (2D) diffraction patterns were obtained using an imaging plate (IP) system (BAS2500, Fuji-Film Co., Japan) [24]. The IP was a digital X-ray film. Subsequently, the 2D data were converted into 1D intensity data to minimize the preferred orientation on the Debye rings. To eliminate air scattering, a vacuum chamber with polyimide (Kapton) film windows was used (125 μm thickness). The pressure was determined from the spectral shift of the R_1 fluorescence line of the ruby balls in the sample chamber of the DAC. The scattered angles, 2θ, and the incident wavelength, λ (=0.08293 nm), were calibrated by using a standard CeO_2 polycrystalline. The scattered wavevector, Q, is represented by $4\pi\sin(\theta)/\lambda$ (nm^{-1}). The crystal structures were analyzed by a combination of *FOX* [25] and *Conograph* [26]. First, *Conograph* was used to calculate the possible lattice parameters and space groups. Then, global optimization by *FOX* identified the space group.

An NRS-5100 Raman Spectrometer (JASCO Co.) equipped with a monochromator and a Peltier-cooled camera was used for the measurements. The excitation was triggered by a 5.8 mW green laser (wavelength of 532 nm).

DFT calculations were performed to assess the interactions between the cations and anion with Raman bands assigned to the molecular vibrations. The conformations of the cations and $[PFBS]^-$ were optimized by DFT. All DFT calculations were performed using the B3LYP hybrid functional and 6–31++G(d,p) basis set of the *Firefly* package [27,28].

3. Results and discussion

3.1. Irreversible phase behavior of [C_4mim][PFBS]

Fig. 1(a) and 1(b) show the X-ray diffraction patterns of [C_4mim][PFBS] at room temperature upon compression and decompression, respectively. Liquid [C_4mim][PFBS] crystallized at 0.3 GPa, named here as the HP- α phase. X-ray structural analysis indicated that the HP- α phase was triclinic ($P\bar{1}$) (Table 1). For comparison, the liquid density of [C_4mim][PFBS] was 1.473 (g cm^{-3}) [29], and the LT crystal density (LT-II phase) was 1.520 (g cm^{-3}) [18]. The HP- α phase is characterized by large lattice constants. The number of cation – anion pairs in the unit cell (Z) was 18. Moreover, the *trans* and *gauche* conformers of $[PFBS]^-$ appeared in the large crystal structure (Fig. 2(a)). The conformer ratio of $[PFBS]^-$ was *trans:gauche* = 8:1 at 0.3 GPa and mixing of the conformers enlarged the unit cell of [C_4mim][PFBS]. In Fig. S1(a), the $[C_4mim]^+$ cation conformers in the unit cell are displayed. *Gauche* cation partially appeared at 0.3 GPa.

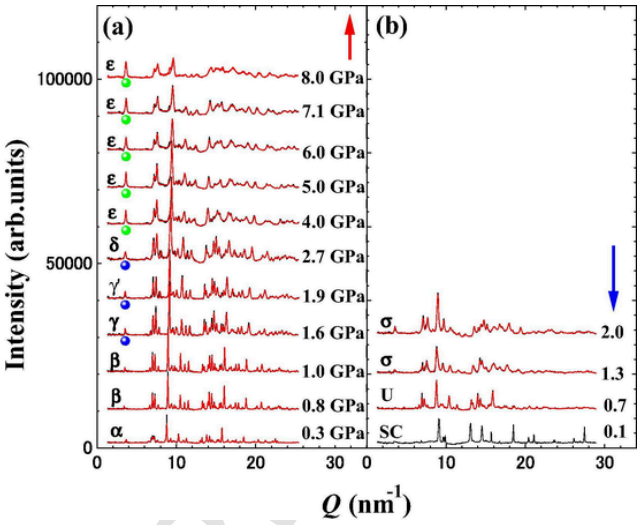

Fig. 1. X-ray diffraction patterns of 1-butyl-3-methylimidazolium perfluorobutanesulfonate ([C_4mim][PFBS]) upon (a) compression and (b) decompression. Black and red curves reveal the observed and calculated patterns, respectively. U and SC reveal unknown phase and single crystal phase, respectively.

Further compression caused a solid – solid phase transition at 0.8 GPa, in which the HP- α phase transformed to the HP- β phase. The transition changed the lattice constants (Table 1), although the space group of the HP- β phase remained the same. In the α- β phase transition, the $[PFBS]^-$ conformer ratio changed a little (for the HP- β phase *trans:gauche* = 6:1) (Fig. 2(b)). Notably, the LT-crystal structure was characterized only by *trans* conformer of $[PFBS]^-$ [18]. Therefore, the presence of *trans* and *gauche* is considered as a pressure effect. Also, the *gauche* conformer ratio of the $[C_4mim]^+$ cation increased at 0.8 GPa (Fig. S1(b)). In the unit cell, two types of the gauche conformers existed. The HP- β phase was also observed at 1.0 GPa. The space group and the conformational ratio at 1.0 GPa were the same as at 0.8 GPa (Table 1).

Phase transition occurred on further compression. At 1.6 GPa ($=P_C$), a new Bragg reflection at low Q (3.56 nm^{-1}) appeared on the

Table 1
Crystallographic data for 1-butyl-3-methylimidazolium perfluorobutanesulfonate ([$C_n$mim][PFBS] (n = 4 and 6)).

[C_4mim][PFBS]			a (nm)	b (nm)	c (nm)	α(°)	β(°)	γ(°)	Z	ρ(g/cm^3)	R_w (%)	R (%)
0.3	α	$P\bar{1}$	1.0277	2.5396	3.4359	80.542	83.518	71.513	18	1.565	10.82	11.70
0.8	β	$P\bar{1}$	2.3450	1.9699	1.9837	71.558	82.238	73.033	18	1.577	9.70	8.74
1.0	β	$P\bar{1}$	2.3399	1.9594	1.9759	71.438	82.068	73.014	18	1.597	7.85	6.95
1.6	γ	C2/c	3.5477	2.0335	1.8597	90	93.642	90	30	1.631	13.09	12.29
1.9	γ'	C2/c	3.5659	2.1262	1.8056	90	100.04	90	30	1.620	15.11	12.48
2.7	δ	C2/m	3.5546	1.0549	1.8034	90	99.287	90	15	1.636	12.42	11.45
4.0	ε	C2	1.7668	0.7183	1.7493	90	99.256	90	5	1.661	11.15	9.55
5.0	ε	C2	1.7621	0.7160	1.7393	90	99.352	90	5	1.680	12.65	10.84
6.0	ε	C2	1.7623	0.7158	1.7373	90	99.250	90	5	1.682	11.61	10.66
7.1	ε	C2	1.7656	0.7118	1.7404	90	99.388	90	5	1.686	13.01	11.99
8.0	ε	C2	1.7602	0.7073	1.7368	90	98.618	90	5	1.702	15.17	14.04
2.0	σ		1.2964	1.8470	1.7696	90	93.867	90	9	1.549	7.78	7.38
1.3	σ		1.2956	1.8489	1.7651	90	94.021	90	9	1.553	14.08	12.48

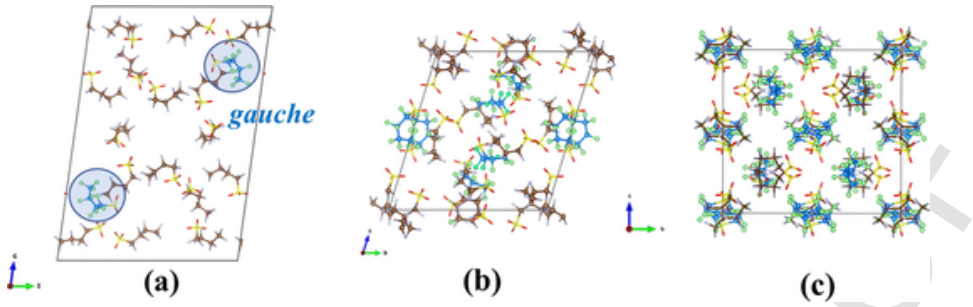

Fig. 2. Unit cells of1-butyl-3-methylimidazolium perfluorobutanesulfonate ([C_4mim][PFBS]) of (a) α phase (0.3 GPa), (b) β phase (0.8 GPa) and (c) γ phase (1.6 GPa). [C_4mim]$^+$ was omitted to enhance the conformers of [PFBS]$^-$. Blue and green colored molecules reveal the *gauche* conformer of [PFBS]$^-$.

X-ray diffraction pattern (blue closed circle in Fig. 1(a)), which indicated a new phase named here as the HP- γ phase. The new peak at low *Q* corresponds to large lattice constants. Through structure analysis, the largest lattice constant was found to be 3.5477 nm, and the space group was determined to be monoclinic (C2/c) (Table 1). The triclinic – monoclinic phase transition at P_C caused the large unit cell, which permitted the lattice modulation. The structure analysis suggests that the *gauche* conformer ratio increased (Fig. 2 (c)) and the ratio of the HP- γ phase was *trans*:*gauche* = 1:1. Hence, in the β- γ (triclinic-monoclinic) phase transition, the *gauche* conformer increased the packing efficiency. Focusing the cation conformers in the HP crystal, the cationic *gauche* conformer ratio exceeded that of the cationic *trans* one (Fig. S1(c)). Consequently, *gauche* conformations both of cation and anion were preferred under HP. On further compression at 1.9 GPa, the β angle changed, although the lattice constants and space group (C2/c) remained the same as at 1.6 GPa (Table 1). Thus, we call the modified phase HP- γ' phase. The conformational ratio of *trans*:*gauche* = 1:1 at 1.9 GPa remained the same as at 1.6 GPa. The crystal morphology was visibly changed at 2.7 GPa under observation through an optical microscope. At 2.7 GPa, peak broadening was dominant particularly at high *Q* region (Fig. 1). Bragg reflections at high *Q* region contain information of intramolecular geometry. Thus, it is difficult to estimate molecular conformations both of cation and anion. In fact, the intermediate conformations, which are distinguished as neither *trans* nor *gauche*, existed in the unit cell of the HP-δ phase. Thus, the conformational ratio of [PFBS]$^-$ was not estimated. Crystal structure analysis without the molecular conformations showed that *b* became half the value at 1.9 GPa and the space group was C2/m (Table 1). The new phase was named the HP-δ phase, and still possessed a large *a* value (Fig. 2(d)). The HP- δ phase was characterized by the loss of the screw axis.

On further compression, a drastic phase change occurred at 4.0 GPa. Analysis of the X-ray diffraction pattern indicated the subsequent phase transition by a change in the peak at low *Q* (green circle in Fig. 1(a)). The peak shifted to 3.67 nm^{-1}, and the peak intensity increased discontinuously. Crystal structure analysis revealed that an entirely different crystal structure (HP- ε phase) had formed at 4.0 GPa. The peak shift at the lowest *Q* position indicates shorter *a* and *b* values (Table 1) and the space group of the HP- ε phase was found to be C2. Furthermore, a further broadening of the Bragg reflections was observed above 4.0 GPa. Conformations in the unit cell were not determined uniquely due to the broad Bragg reflections. From 4.0 to 8.0 GPa, no phase transitions were observed. During the entire compression process, complicated crystal polymorphs such as α, β, γ, γ',δ and ε phases were observed and were interpreted by introducing the crystal energy landscape [2]. Compared with the HP phase behaviors of [C_4mim][PF_6] [30], partial amorphization was not observed in [C_4mim][PFBS].

Upon decompression, the HP- σ phase, for which the space group was $P2_1$, appeared at 2.0 GPa. The peak intensity at the lowest *Q* position weakened. The lattice parameters of the HP- σ phase are listed in Table 1. Notably, the HP- σ phase was different from those found upon compression (i.e. the α, β, γ, γ',δ and ε phases). We cannot determine the space group of the complicated HP- σ phase even by so many trials of the structural determinations. Thus, HP single-crystal X-ray diffraction could be requited for further structure analysis [31]. Considering the compression and decompression processes, the irreversible phase transition of [C_4mim][PFBS] was induced under HP. Upon decreasing the pressure, the HP- σ phase existed even at 1.3 GPa. At 0.7 GPa, a new decompression phase was detected, which was indicated by changes in the X-ray diffraction pattern (Fig. 1(b)). However, the new phase structure was not resolved owing to the preferred orientation of the Bragg reflections. Thus, we named unknown phase (HP-U phase). Just before melting, the phase transition from a polycrystal to a single crystal (SC) phase occurred at 0.1 GPa. Typical sharp Bragg spots were monitored on the IP. Thus, the crystal structure was not determined. We predict that the crystal structure at 0.1 GPa is one of the LT phases [18].

The HP crystal polymorph is schematically illustrated in addition to the LT crystal polymorph in Fig. 3. Compared with the LT crystal polymorph, the HP crystal polymorph was complicated and irreversible upon compression and decompression. Nevertheless, the crystallographic features of [C_4mim][PFBS] are described by the large lattice constant both at LT [18] and HP (Table 1). In the case of [C_4mim][PF_6], LT and HP crystal polymorphs were also observed. Particularly, the LT- β phase [32] and the HP- β phase [30] possessed a large lattice

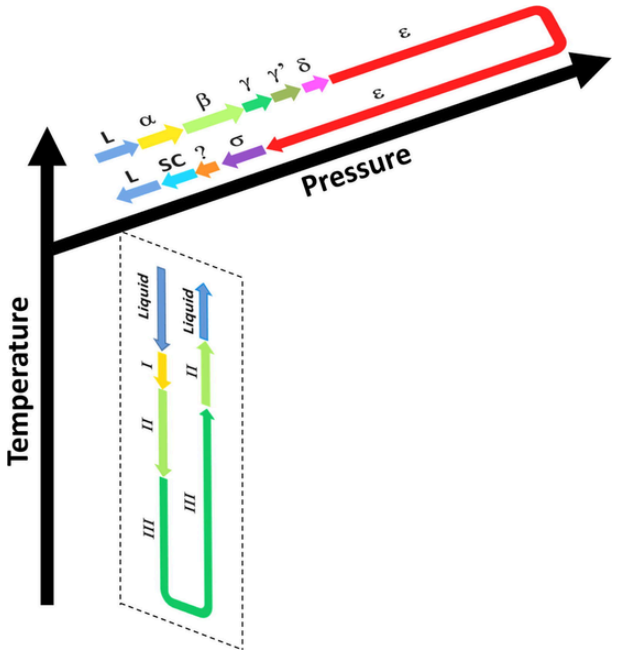

Fig. 3. Schematic crystal polymorphs of 1-butyl-3-methylimidazolium perfluorobutanesulfonate ([C_4mim][PFBS])at LT and HP.

constant for [C_4mim][PF_6]. In the LT- β phase of [C_4mim][PF_6], the *TT* conformer of [C_4mim]$^+$ was identified using Raman spectroscopy [33]. Moreover, [PFBS]$^-$ conformers in crystals cause the different crystal lattices at LT and HP. LT-crystals of [C_4mim][PFBS] consist only of *trans* conformer of [PFBS]$^-$ [18], although the *gauche* conformers of [PFBS]$^-$ were formed under HP. Conformation-driven molecular orientational and positional orders are quite sensitive to the molecular packing, which determines the crystal lattices. Generally, crystal structures in the molecular system are directly connected with their molecular conformations. Conformational varieties relating to the crystal polymorphs could be explained by the crystal energy landscape.

3.2. Conformational changes of [C_4mim]$^+$

HP Raman spectroscopy experiments were performed to investigate the relationship between molecular conformation and crystal structure. Fig. 4 indicates the Raman spectra of the CH_2 rocking mode of [C_4mim]$^+$ upon compression. The Raman bands were separated using profile fitting of the asymmetric pseud-Voigt function. At ambient pressure (0.1 MPa), *trans* and *gauche* conformers coexisted. The *gauche* conformer ratio was a little larger than the *trans* one in the liquid. Even at 0.16 GPa, the super-pressurized liquid was present with almost the same conformational ratio and positions. Using optical microscope observation, crystal domains were formed immediately at 0.2 GPa. Once crystallization of the HP- α phase occurred, the Raman bands became sharper (Fig. 4). Moreover, the broad *gauche* band at 0.16 GPa decomposed into three bands at 0.2 GPa. In addition to *GT* and *G'T*, a new Raman band appeared at the lower position. This result did not contradict with small ratio of the *gauche* conformer of [C_4mim]$^+$ in the unit cell of the HP- α phase (Fig. S1(a)). However, the three types of the *gauche* conformers were not distinguished by crystal structure analysis.

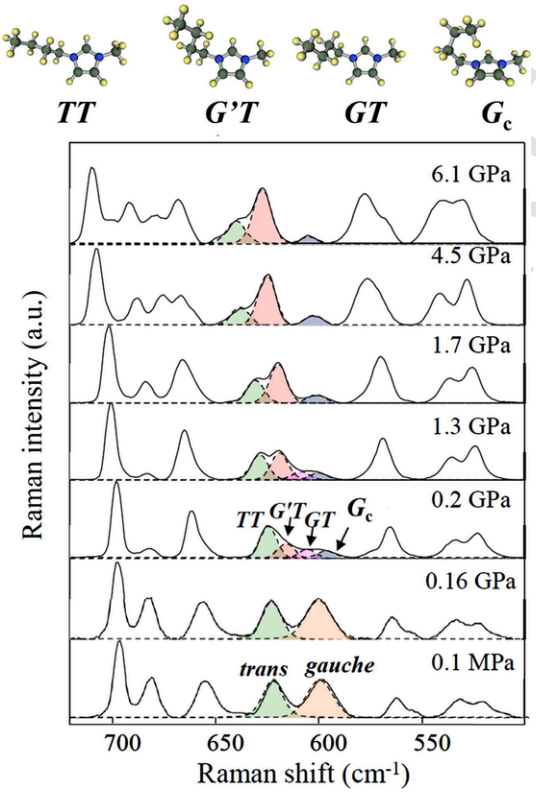

Fig. 4. Raman bands of 1-butyl-3-methylimidazolium ([C_4mim]$^+$) as a function of pressure. *TT* corresponds to *trans*, and *GT*, *G'T*, and G_c belong to *gauche*. Each conformer is assigned by the CH_2 rocking mode of [C_4mim]$^+$.

Similar to the HP crystal polymorph of [C_4mim][PF_6] [30], the lowest positioned *gauche* corresponds to the spatially constrained gauche (G_c). The G_c could be a folding conformer, resembling the *ng'g* conformer in the literature [17]. The calculated Raman bands of [C_4mim]$^+$ were indicated in Fig. 10(c) and Fig. S3 of the reference [17], and the four *gauche* conformers were identified separately. For high packing efficiency under HP, the folded G_c conformer is HP-inherent. In the case of [C_4mim][PF_6], with increasing pressure, the gradual increment of the G_c conformer was directly connected with partial amorphization [30]. With increasing pressure, the *GT* conformer of [C_4mim][PFBS] became small, although *G'T* increased at 1.3 GPa. Considering the X-ray diffraction patterns at 0.8 and 1.0 GPa, the conformational change corresponds to the α - β phase transition. Crystal structure of the HP- β phase indicates an increment of the *gauche* conformer of [C_4mim]$^+$ at 0.8 GPa (Fig. S1(b)). *Gauche* increment by X-ray diffraction is consistent qualitatively with that by Raman spectroscopy. At 1.7 GPa (P_C), the *GT* Raman band completely disappeared accompanied by the β - γ phase transition. While, the *G'T* Raman band at P_C exceeded the *TT* Raman band as shown in Fig. 4. Considering the crystal structure of the HP- γ phase at 1.6 GPa (Fig. S1(c)), the *trans* and *gauche* ratio of [C_4mim]$^+$ in the unit cells can explain the Raman intensity ratio of *TT* and *G'T*. Above 2 GPa, the *TT* Raman band of [C_4mim]$^+$ gradually decreased with preferring packing efficiency. Inversely *G'T* gradually developed. Above 2 GPa, the distinct changes of the cationic Raman bands were not observed.

The pressure dependence of peak positions of the [C_4mim]$^+$ conformers is plotted in Fig. 5(a). *Gauche* conformers drastically changed at each phase transition under HP. This means that *gauche* conformers are sensitive to the cation–anion pairing in the unit cells. DFT calculations indicate an anion dependence of the [C_4mim]$^+$ conformers (Fig. S2). The calculated peak positions of the *trans* conformer were not significantly shifted according to the type of anion. In contrast, the *GT* and *G'T* conformers were influenced by the anion species. The DFT calculations imply that the ion-pairing changed extensively in the α crystallization and α- β and β- γ phase transitions. Another approach to interpreting the HP phase behaviors of [C_4mim][PFBS] is the conformational ratios of [C_4mim]$^+$. The intensity fraction, f_i, of the [C_4mim]$^+$ conformer is provided by;

$$f_i = \frac{I_i}{I_{TT} + I_{GT} + I_{G'T} + I_{Gc}} \quad (1)$$

in which I_{TT}, I_{GT}, $I_{G'T}$ and I_{Gc} are intensities of Raman bands. In Fig. 5(b), f_i upon compression is indicated. A series of phase changes such as liquid- α - β – γ- γ ' below 3 GPa are well described by the changing in their conformations. When the HP- γ phase appeared at 1.7 GPa (P_C), the *GT* conformer vanished. As shown in Fig. 4, the molecular structure of the *GT* conformer is not adequate geometrically for the higher packing conditions. Thus, we confirm that *GT* transformed to *G'T* in the β- γ phase transition. From 0.2 GPa to P_C, the *TT* conformer of [C_4mim]$^+$ decreased monotonically, whereas *G'T* exceeded $f_{G'T} = 0.6$ at approximately 2 GPa. Molecular packing was compensated mainly by the folding alkyl chain of [C_4mim]$^+$ below P_C. Above 3 GPa, the conformational ratio of *TT* and *G'T* did not change at all. Hence, the cation folding saturated at approximately P_C, and the invariant *G'T* conformer above P_C implies that the cation conformers did not contribute to the densely packed conditions. On the other hand, the G_c conformer was almost constant over the whole pressure region. As partial amorphization of [C_4mim][PF_6] was induced by an increase of the G_c conformer, no amorphization of [C_4mim][PFBS] is explained by the constant G_c ratio up to P_{max}.

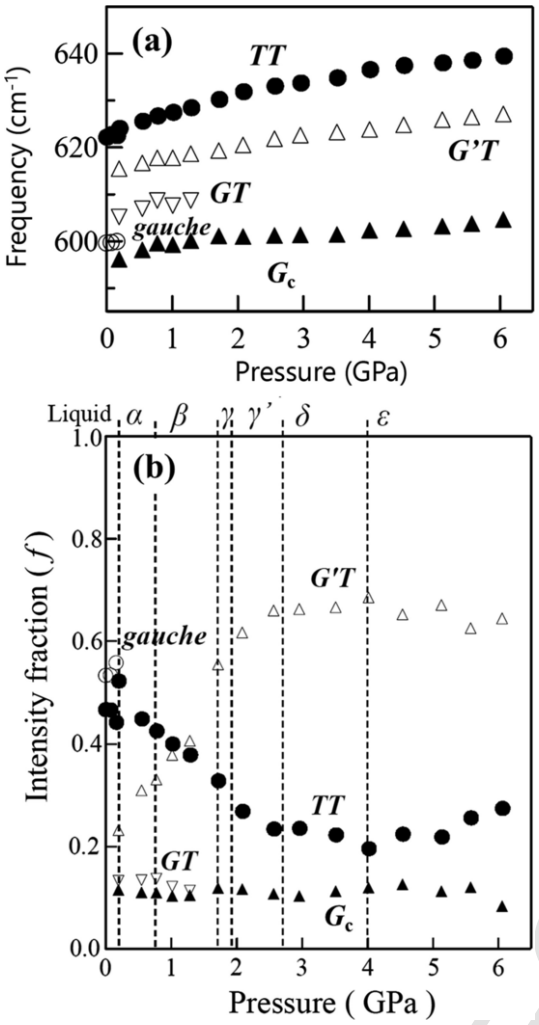

Fig. 5. Pressure dependences of 1-butyl-3-methylimidazolium ($[C_4mim]^+$) conformations on (a) peak positions, and (b) intensity fraction, f_i.

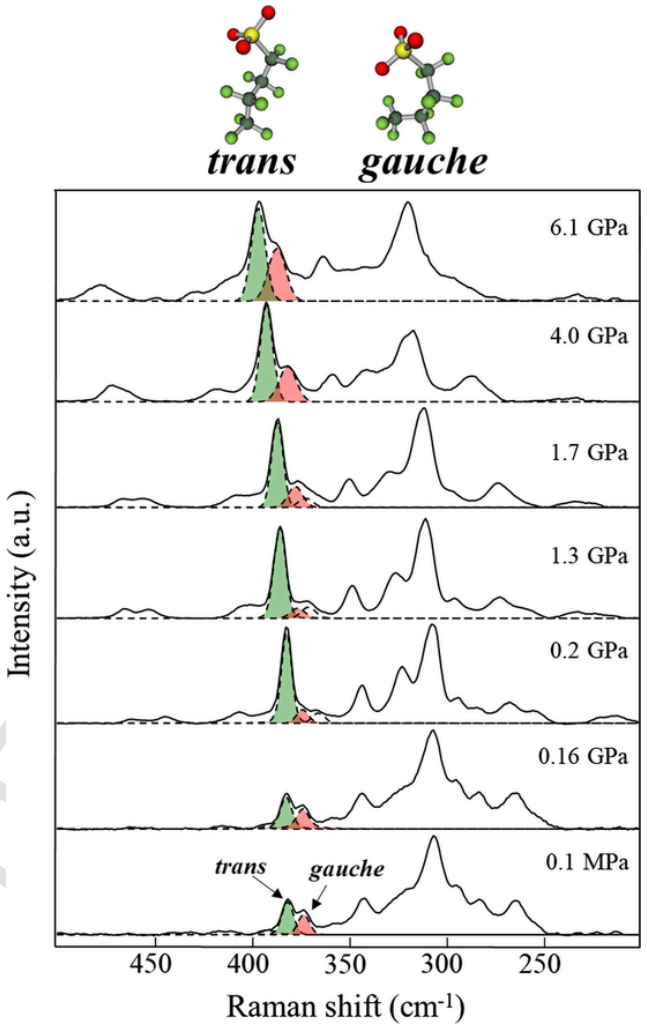

Fig. 6. Raman spectra of the SO_3 wagging mode of perfluorobutanesulfonate ($[PFBS]^-$). The trans and gauche conformers are identified by the respective density functional theory calculations.

3.3. Conformational changes of [PFBS]$^-$

The torsional potential of $[PFBS]^-$ was estimated using DFT calculations [18]. It was found that the *trans* and *gauche* conformers of $[PFBS]^-$ are stabilized. In this study, Raman bands of the -SO_3 wagging mode were used to assign the *trans* and *gauche* conformations of $[PFBS]^-$ using DFT. Fig. 6 reveals a dependence between pressure and the Raman bands of $[PFBS]^-$. In Fig. S3, all Raman spectra upon compression are indicated. The observed peaks were decomposed by the asymmetric profile fitting. The liquid at 0.1 MPa and the super-pressurized liquid at 0.16 GPa have the same Raman spectra. At 0.2 GPa, the *trans* Raman band of $[PFBS]^-$ increased, which was accompanied by crystallization, and is consistent with the unit cell, which mainly consisted of the *trans* conformer (Fig. 2(a)). The conformational ratio of *gauche* increased relatively with pressure. The tendency coincided with an increase in the *gauche* conformer of $[PFBS]^-$ in the unit cell indicated by X-ray diffraction analysis.

For a quantitative analysis of the anion conformers, the intensity fractions, f_i, are exhibited in Fig. 7. Crystallization at 0.2 GPa caused an abrupt increase in the *trans* conformer of $[PFBS]^-$. This is similar to the sudden conformational change of $[C_4mim]^+$. In contrast, in the triclinic α and β phases, opposite behaviors between the cation and anion were observed. Small changes in the anion conformers were observed below 1.7 GPa (P_C), whereas the cation conformations varied below P_C. Hence, a volume contraction below P_C was realized owing to the cation folding. More importantly, drastic jumps of intensity fractions were induced by the monoclinic HP- γ phase appearance at 1.7 GPa (P_C). At P_C, the crystal system varied from triclinic to monoclinic, and the phase transition promoted molecular rearrangements (Fig. 2(b) and 2(c)). Simultaneously, the *trans* and *gauche* ratio of $[PFBS]^-$ changed extensively (Fig. 7). Here, we summarize the pressure dependency of the conformational variances, which relate to the crystal system as follows:

(i) Crystal system: triclinic ($P < P_C$), monoclinic ($P_C < P$)
(ii) Cation: variant ($P < P_C$), invariant ($P_C < P$)
(iii) Anion: invariant ($P < P_C$), variant ($P_C < P$)

In the pressure-driven conformational changes, the switching effect at P_C is significant in addition to the disappearance of the *GT* cation conformer at P_C. If we assume that $[C_4mim]^+$ is more flexible than $[PFBS]^-$, the switching effect is explained. At first, folding of the flexible $[C_4mim]^+$ was favored for a volume contraction below P_C. After saturation of cation folding, the relatively inflexible $[PFBS]^-$ changed its conformation in the densely packed conditions above P_C. It should be noticed that, in the gas state, torsion potential energy profiles of $[C_4mim]^+$ were provided in Fig. 3 of the reference [14]. The rota-

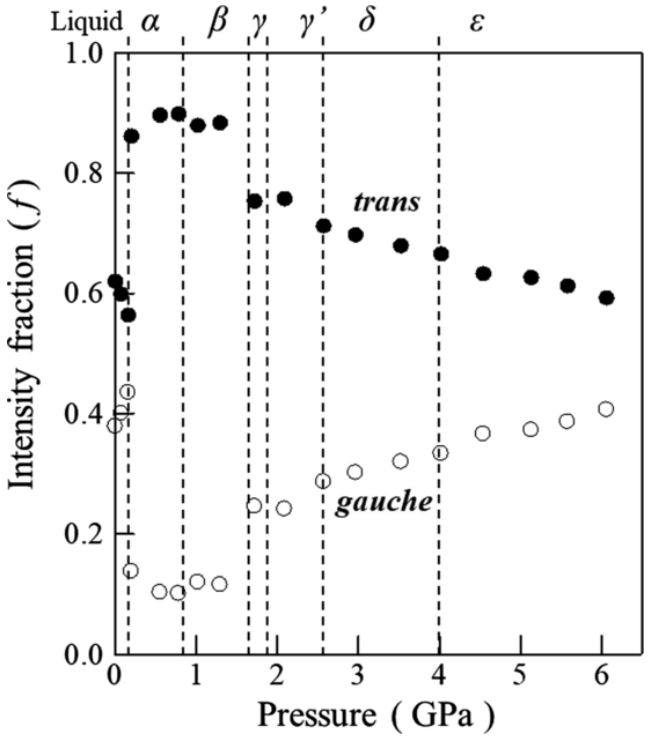

Fig. 7. Intensity fractions, f_i, of perfluorobutanesulfonate ([PFBS]$^-$) as a function of pressure.

tional barriers of the isolated cation were estimated to be 19 kJ/mol and 15 kJ/mol by the DFT calculations. On the other hand, the barrier of isolated [PFBS]$^-$ was found to be 6.3 kJ/mol [18]. Generally, the low energy barrier causes (i) conformational flexibility, (ii) fast dynamics between *trans* and *gauche*, (iii) increasing entropy, (iv) high activation volume, (v) low viscosity, and (vi) high conductivity [34]. In fact, macroscopic properties of [C$_n$mim][PFBS] are explained by the low barrier [20,21,29]. As shown in Fig. 6, *trans* and *gauche* Raman intensities of [PFBS]$^-$ in the liquid (0.16 GPa) were comparable due to the fast dynamics of *trans-gauche* interconversion. When the HP-crystallization occurred at 0.2 GPa, *trans* Raman band increased drastically. We predict that, by HP-crystallization, large free volume of [PFBS]$^-$ in the liquid state is reduced, and the barrier between *trans* and *gauche* becomes much larger. Then, flexibility of [PFBS]$^-$ was lost above 2.0 GPa). On the other hand, in [C$_4$mim]$^+$, equimolar mixture of *trans* and *gauche* in the liquid (Fig. 4) was almost maintained after the HP-crystallization. Hence, conformational flexibility of [C$_4$mim]$^+$ could be sustained even after the HP-crystallization. Above P_C, a monotonic increase of the *gauche* conformer of [PFBS]$^-$ was observed with increasing pressure. As the shape of the *gauche* conformer of [PFBS]$^-$ is spherical as shown in Fig. 6, molecular packing efficiency could be improved by an increment of the *gauche* fraction. Also, a molecular orientational disorder of [PFBS]$^-$ could develop above P_C due from the increase of the *gauche* conformer of [PFBS]$^-$. The disorder such as plastic crystal does not contradict with the HP phase transitions.

In the case of [C$_4$mim][PF$_6$], the G_c conformer of [C$_4$mim]$^+$ increased markedly, as [PF$_6$]$^-$ has no degrees of freedom of conformations. Partial amorphization was induced by the cationic disorder of G_c in [C$_4$mim][PF$_6$]. Compared with the HP-phase behaviors of [C$_4$mim][PF$_6$], [PFBS]$^-$ has an adjusting mechanism for volume contraction with increasing the *gauche* conformer of [PFBS]$^-$. Therefore, a combination of cation folding and anion adjusting could suppress an increase in the G_c cation conformer and the partial amorphization in [C$_4$mim][PFBS].

4. Summary

The phase behaviors of [C$_4$mim][PFBS] under HP were observed using X-ray diffraction and Raman spectroscopy. The HP crystal polymorph of the fIL was irreversible upon compression and decompression. The flexible [C$_4$mim]$^+$ tended to fold gradually with the invariant anion conformer below P_C. Once the *gauche* conformer of the cation was saturated at P_C, the anion conformers became the variant above P_C. At the switching pressure, the triclinic-monoclinic phase transition occurred. In contrast to the no degrees of freedom of the anionic conformations, such as in [PF$_6$]$^-$, the variable conformations of [PFBS]$^-$ between *trans* and *gauche* prevent an increment of the G_c conformer of [C$_4$mim]$^+$ and partial amorphization. The HP-crystal polymorph based on the cationic and anionic conformational varieties supports a concept of the crystal energy landscape.

CRediT authorship contribution statement

Yoshihiro Koyama: Data curation, Formal analysis. **Seiya Shimono:** Data curation. **Hiroaki Kishimura:** Data curation. **Takahiro Takekiyo:** Data curation, Formal analysis. **Yukihiro Yoshimura:** Supervision. **Hiroshi Abe:** Conceptualization, Writing - original draft, Writing - review & editing. **Kiyoto Matsuishi:** Supervision.

Declaration of Competing Interest

The authors declare that they have no known competing financial interests or personal relationships that could have appeared to influence the work reported in this paper.

Acknowledgments

We appreciate Prof. N. Hamaya of Ochanomizu University and Prof. A. Shimizu of Soka University for helpful discussions.

Appendix A. Supplementary material

Supplementary data to this article can be found online at https://doi.org/10.1016/j.molliq.2021.116415.

References

[1] B.A. Nogueira, C. Castiglioni, R. Fausto, Color polymorphism in organic crystals, Commun. Chem. 3 (2020) 34–112.
[2] S.L. Price, Why don't we find more polymorphs?, Acta Cryst. B 69 (2013) 313–328.
[3] G.J.O. Beran, Modeling Polymorphic Molecular Crystals with Electronic Structure Theory, Chem. Rev. 116 (2016) 5567–5613.
[4] P.M. Piaggia, M. Parrinellob, Predicting polymorphism in molecular crystals using orientational entropy, Proc. Nat. Acad. Soc. 115 (2018) 10251–10256.
[5] M.A. Neumann, J. van de Streek, F.P.A. Fabbiani, P. Hidber, O. Grassmann, Combined crystal structure prediction and high-pressure crystallization in rational pharmaceutical polymorph screening, Nature Commun. 6 (2015) 7793–7797.
[6] J. Hoja, H.-Y. Ko, M.A. Neumann, R. Car, R.A. DiStasio Jr., A. Tkatchenko, Reliable and practical computational description of molecular crystal polymorphs, Sci. Adv. 5 (2019) 3338–3339.
[7] A.J. Cruz-Cabeza, E. Taylor, I.J. Sugden, D.H. Bowskill, S.E. Wright, H. Abdullahi, D. Tulegenov, G. Sadiq, R.J. Davey, Can solvated intermediates inform us about nucleation pathways? The case of β-pABA, CrystEngComm 22 (2020) 7447–7459.
[8] A. Johnston, A.J. Florence, N. Shankland, A.R. Kennedy, K. Shankland, S.L. Price, Crystallization and Crystal Energy Landscape of Hydrochlorothiazide, Cryst. Growth Des. 7 (2007) 705–712.
[9] S.L. Price, From crystal structure prediction to polymorph prediction: interpreting the crystal energy landscape, Phys. Chem. Chem. Phys. 10 (2008) 1996–2009.
[10] S.Z. Ismail, C.L. Anderton, R.C.B. Copley, L.S. Price, S.L. Price, Evaluating a crystal energy landscape in the context of industrial polymorph screening, Cryst. Growth Des. 13 (2013) 2396–2406.
[11] S.L. Price, D.E. Braun, S.M. Reutzel-Edens, Can computed crystal energy landscapes help understand pharmaceutical solids?, Chem. Commun. 52 (2016) 7065–7077.

[12] S.L. Price, S.M. Reutzel-Edens, The potential of computed crystal energy landscapes to aid solid-form development, Drug Discovery Today 21 (2016) 912–923.
[13] P.G. Debenedetti, F.H. Stillinger, Supercooled liquids and the glass transition, Nature 410 (2001) 259–267.
[14] J.N. Canongia Lopes, J. Deschamps, A.A.H. Pádua, Modeling Ionic Liquids Using a Systematic All-Atom Force Field, J. Phys. Chem. B 108 (2004) 2038–2047.
[15] S. Tsuzuki, A.A. Arai, K. Nishikawa, Conformational analysis of 1-Butyl-3-methylimidazolium by CCSD(T) Level Ab Initio Calculations: Effects of Neighboring Anions, J. Phys. Chem. B 112 (2008) 7739–7747.
[16] J. Kiefer, C.C. Pye, Structure of the Room-Temperature Ionic Liquid 1-Hexyl-3-methylimidazolium Hydrogen Sulfate: Conformational Isomerism, J. Phys. Chem. A 114 (2010) 6713–6720.
[17] T. Endo, T. Higuchi, Y. Kimura, DFT study on conformation of 1-Alkyl-3-methylimidazolium with Ethyl, Propyl, Butyl, Pentyl, and Hexyl Group, Bull. Chem. Soc. Jpn. 93 (2020) 720–729.
[18] Y. Koyama, S. Shimono, H. Abe, K. Matsuishi, Crystal polymorphs in 1-alkyl-3-methylimidazolium perfluorobutanesulfonate ionic liquids, J. Mol. Liq. 317 (2020) 113908–113917.
[19] S. Tsuzuki, T. Umecky, H. Matsumoto, W. Shinoda, M. Mikami, Interactions of Perfluoroalkyltrifluoroborate Anions with Li Ion and Imidazolium Cation: Effects of Perfluoroalkyl Chain on Motion of Ions in Ionic Liquids, J. Phys. Chem. B 114 (2010) 11390–11396.
[20] A.B. Pereiro, M.J. Pastoriza-Gallego, K. Shimizu, I.M. Marrucho, J.N. Canongia Lopes, M.M. Piñeiro, L.P.N. Rebelo, On the formation of a third, nanostructured domain in ionic liquids, J. Phys. Chem. B 117 (2013) 10826–10833.
[21] M.L. Ferreira, M.J. Pastoriza-Gallego, J.M.M. Araújo, J.N. Canongia Lopes, L.P.N. Rebelo, M.M. Piñeiro, K. Shimizu, A.B. Pereiro, Influence of nanosegregation on the phase behavior of fluorinated ionic liquids, J. Phys. Chem. 121 (C 2017,) 5415–5427.
[22] K. Shimizu, A.A. Freitas, J.N. Canongia Lopes, Structural characterization of the $[C_nC_1im][C_4F_9SO_3]$ ionic liquid series: Alkyl versus perfluoroalkyl side chains, J. Mol. Liq. 226 (2017) 28–34.
[23] J. Luo, A.H. Jensen, N.R. Brooks, J. Sniekers, M. Knipper, D. Aili, Q. Li, B. Vanroy, M.W¨ubbenhorst, F. Yan, L. Van Meervelt, Z. Shao, J. Fang, Z.-H. Luo, D.E. De Vos, K. Binnemans, J. Fransaer, 1,2,4-Triazolium perfluorobutanesulfonate as an archetypal pure protic organic ionic plastic crystal electrolyte for all-solid-state fuel cells, Energy Environ. Sci. 8 (2015) 1276–1291.
[24] O. Shimomura, K. Takemura, H. Fujihisa, Y. Fujii, Y. Ohishi, T. Kikegawa, Y. Amemiya, T. Matsushita, Application of an imaging plate to high-pressure x-ray study with a diamond anvil cell, Rev. Sci. Instrum. 63 (1992) 967–973.
[25] V. Favre-Nicolin, R. Cerny, FOX, 'free objects for crystallography': a modular approach to ab initio structure determination from powder diffraction, J. Appl. Cryst. 35 (2002) 734–743.
[26] R. Oishi-Tomiyasu, Robust powder auto-indexing using many peaks, J. Appl. Cryst. 47 (2014) 593–598.
[27] A.A. Granovsky, Firefly version 8, http://classic.chem.msu.su/gran/firefly/index.html.
[28] M.W. Schmidt, K.K. Baldridge, J.A. Boatz, S.T. Elbert, M.S. Gordon, J.H. Jensen, S. Koseki, N. Matsunaga, K.A. Nguyen, S. Su, T.L. Windus, M. Dupuis, J.A. Montgomery Jr., General atomic and molecular electronic structure system, J. Comput. Chem. 14 (1993) 1347–1363.
[29] P. Bonhôte, A.-P. Dias, N. Papageorgiou, K. Kalyanasundaram, M. Gra1tzel, Hydrophobic, highly conductive ambient-temperature molten salts, Inorg. Chem. 35 (1996) 1168–1178.
[30] H. Abe, T. Takekiyo, N. Hatano, M. Shigemi, N. Hamaya, Y. Yoshimura, Pressure-induced frustration–frustration process in 1-Butyl-3-methylimidazolium hexafluorophosphate, a room-temperature ionic liquid, J. Phys. Chem. B 118 (2014) 1138–1145.
[31] N. Hirao, S.I. Kawaguchi, K. Hirose, K. Shimizu, E. Ohtani, Y. Ohishi, New developments in high-pressure X-ray diffraction beamline for diamond anvil cell at SPring-8, Matter Radiat. Extremes 5 (2020) 018403–018410.
[32] S. Saouane, S.E. Norman, C. Hardacre, F.P.A. Fabbiani, Pinning down the solid-state polymorphism of the ionic liquid [bmim][PF_6], Chem. Sci. 4 (2013) 1270–1280.
[33] T. Endo, T. Kato, K. Tozaki, K. Nishikawa, Phase Behaviors of Room Temperature Ionic Liquid Linked with Cation Conformational Changes: 1-Butyl-3-methylimidazolium Hexafluorophosphate, J. Phys. Chem. B 114 (2010) 407–411.
[34] F. Philippi, D. Pugh, D. Rauber, T. Welton, P.A. Hunt, Conformational design concepts for anions in ionic liquids, Chem. Sci. 11 (2020) 6405–6422.